

AD-A113 139

AIR FORCE GEOPHYSICS LAB HANSCOM AFB MA  
IMPROVED 35 MHZ RADIOMETER FOR SOLAR BURST MEASUREMENTS.(U)  
AUG 81 D A GUIDICE, C P FEROLI

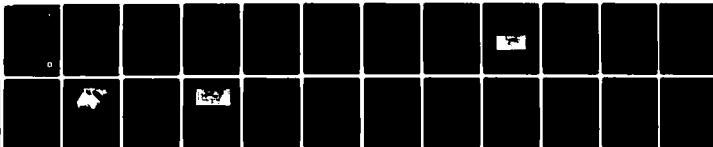
F/O 3/2

UNCLASSIFIED

AFGL-TR-81-0253

NL

For  
Review



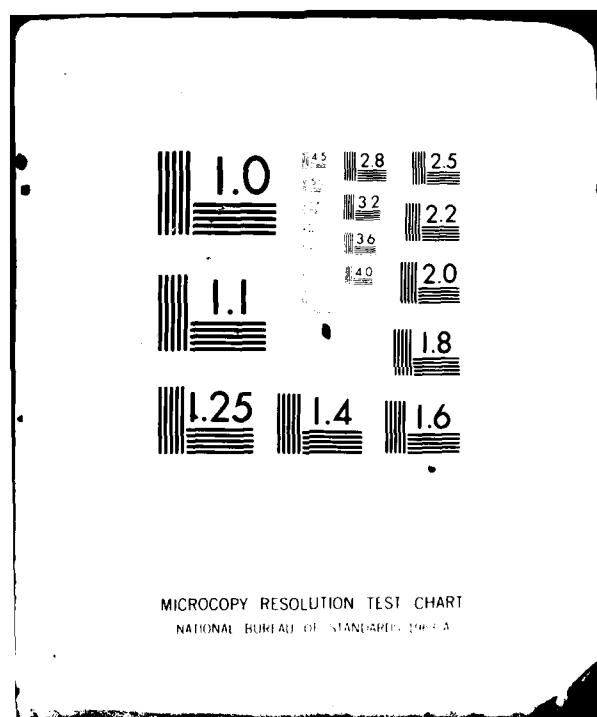
END

DATE

FILED

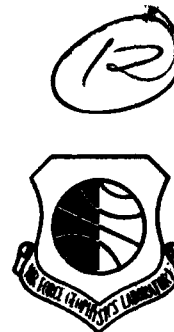
4-82

DTIC



AD A113139

AFGL-TR-81-0253  
INSTRUMENTATION PAPERS, NO. 304



## Improved 35 GHz Radiometer for Solar Bursts Measurements

DONALD A. GUIDICE  
CARL P. FERIOLO

26 August 1981

Approved for public release; distribution unlimited.

SPACE PHYSICS DIVISION PROJECT 4643  
**AIR FORCE GEOPHYSICS LABORATORY**  
HANSCOM AFB, MASSACHUSETTS 01731

**AIR FORCE SYSTEMS COMMAND, USAF**

**DTIC**  
**ELECT**  
**S** APR 7 1982 **D**  
**A**



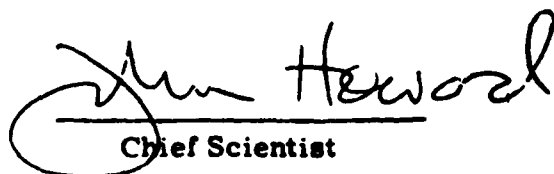
DTIC FILE COPY

82 04 07 043

This report has been reviewed by the ESD Public Affairs Office (PA) and is releasable to the National Technical Information Service (NTIS).

This technical report has been reviewed and is approved for publication.

FOR THE COMMANDER

  
Chief Scientist

Qualified requestors may obtain additional copies from the Defense Technical Information Center. All others should apply to the National Technical Information Service.

Unclassified

SECURITY CLASSIFICATION OF THIS PAGE (When Data Entered)

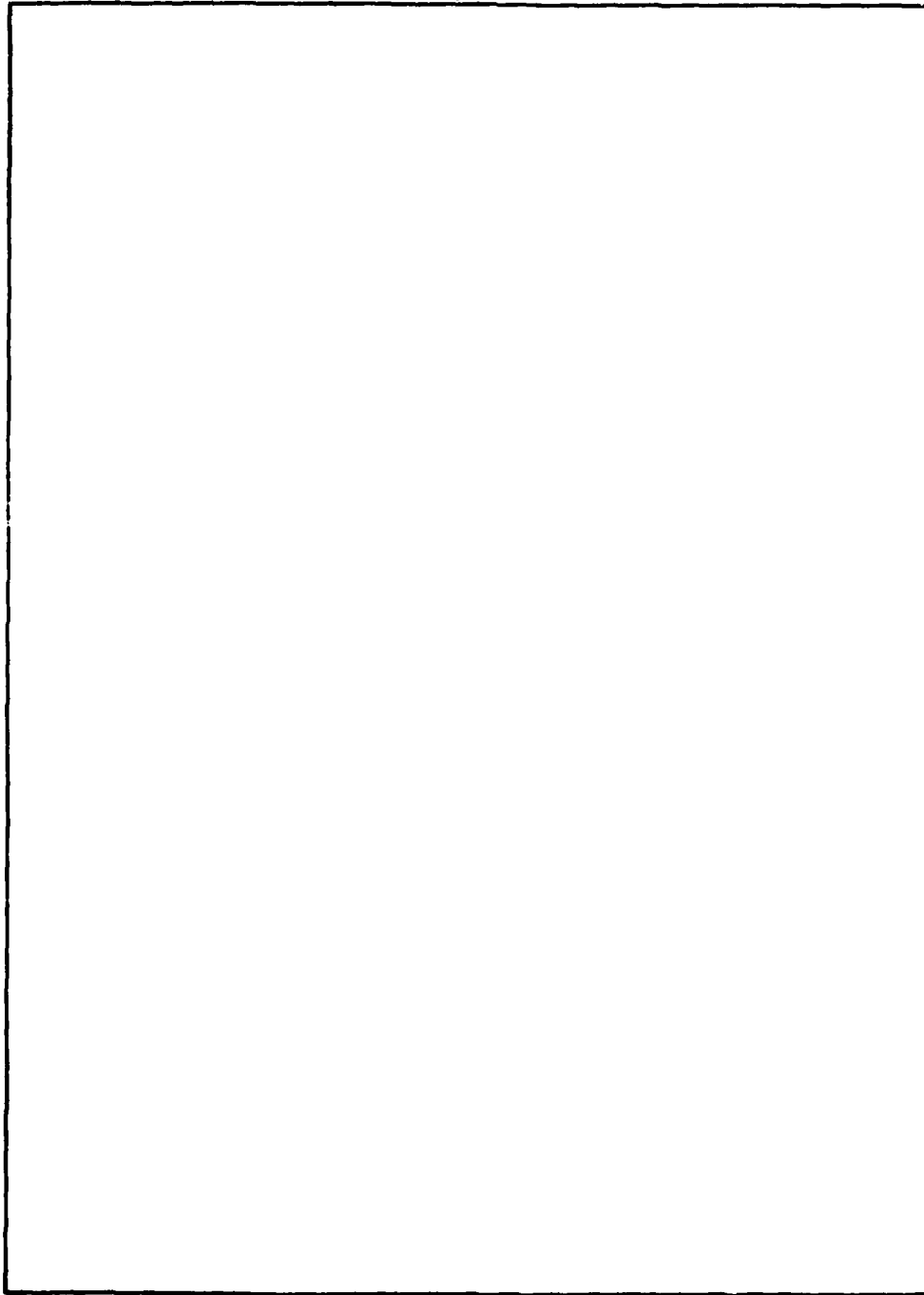
REPORT DOCUMENTATION PAGE		READ INSTRUCTIONS BEFORE COMPLETING FORM
1. REPORT NUMBER AFGL-TR-81-0253	2. GOVT ACCESSION NO. AD-4113	3. RECIPIENT'S CATALOG NUMBER 139
4. TITLE (and Subtitle) IMPROVED 35 GHz RADIOMETER FOR SOLAR BURST MEASUREMENTS		5. TYPE OF REPORT & PERIOD COVERED Scientific, Interim.
		6. PERFORMING ORG. REPORT NUMBER IP No. 304
7. AUTHOR(s) Donald A. Guidice Carl P. Ferioli		8. CONTRACT OR GRANT NUMBER(s)
9. PERFORMING ORGANIZATION NAME AND ADDRESS Air Force Geophysics Laboratory (PHG) Hanscom AFB Massachusetts 01731		10. PROGRAM ELEMENT, PROJECT, TASK AREA & WORK UNIT NUMBERS 62101F 46430308
11. CONTROLLING OFFICE NAME AND ADDRESS Air Force Geophysics Laboratory (PHG) Hanscom AFB Massachusetts 01731		12. REPORT DATE 26 August 1981
		13. NUMBER OF PAGES 27
14. MONITORING AGENCY NAME & ADDRESS (if different from Controlling Office)		15. SECURITY CLASS. (of this report) Unclassified
		15a. DECLASSIFICATION DOWNGRADING SCHEDULE
16. DISTRIBUTION STATEMENT (of this Report)  Approved for public release; distribution unlimited.		
17. DISTRIBUTION STATEMENT (of the abstract entered in Block 20, if different from Report)		
18. SUPPLEMENTARY NOTES		
19. KEY WORDS (Continue on reverse side if necessary and identify by block number) Solar radio bursts                      8-mm wavelength measurements Solar measurements                      Wide bandwidth radiometer 35 GHz radiometer                      Burst spectral development		
20. ABSTRACT (Continue on reverse side if necessary and identify by block number) ✓ The new 35-GHz patrol radiometer at Sagamore Hill Radio Observatory is described. The improved sensitivity of this system permits the detection of solar bursts down to about a 5-10 sfu level vs 50-100 sfu for the old system. This enhanced sensitivity will aid in the investigation of a wide range of topics pertaining to the physics of solar flares. These include but are not limited to spectral studies of large flare-bursts, correlations with hard x-ray data, and the detection of short cm-λ sharp-cutoff bursts.		

DD FORM 1 JAN 73 1473

Unclassified

SECURITY CLASSIFICATION OF THIS PAGE (When Data Entered)

SECURITY CLASSIFICATION OF THIS PAGE(When Data Entered)



SECURITY CLASSIFICATION OF THIS PAGE(When Data Entered)

## Preface

The authors are indebted to Mr. John Castelli for his development of the instrumentation for fixed-frequency whole-sun patrol observations at the Sagamore Hill Radio Observatory. This instrumentation served as the general model for the improved 35-GHz radiometer we developed. We thank Mr. Castelli for his outstanding leadership of the solar radio measurements program at Sagamore Hill over its many years of operation and for his continuing interest in short-centimeter and millimeter wavelength solar observations. The authors also acknowledge the continuing support of solar radio measurements and their use in forecasting burst-induced terrestrial effects by Dr. Jules Aarons, chief of the Trans-Ionospheric Propagation Branch.



DTIC	DTIC
COPY	COPY
INSPECTED	INSPECTED
2	2

## Contents

1. INTRODUCTION	7
2. RADIOMETER IMPROVEMENTS	10
2.1 Design Improvements	10
2.2 Block Diagram and Wiring Diagrams	13
2.3 Sensitivity Calculations for the New System	14
3. NEW CAPABILITIES	20
3.1 For the 35 GHz Patrol	20
3.2 For the Solar Radio Patrol as a System	21
3.2.1 Time Development of Spectra of Selected Large Bursts	21
3.2.2 Time Development of Spectra of Many Simple Bursts	22
3.2.3 Correlation of Hard X-ray Spectra With Microwave Spectra	22
3.2.4 High-Frequency Sharp-Cutoff Bursts	23
4. CONCLUSIONS	23
APPENDIX A: 35 GHz Solar Radiometer Parts List	25

## Illustrations

1. A View of the Sagamore Hill Solar Radio Patrol Station	8
2. Upper Level of Largest Burst Flux Density Over the Microwave Range in Comparison to Quiet-Sun Flux Densities	9
3. Block Diagram of the Improved 35-GHz Radiometer	14

## Illustrations

4. Photograph Showing the Instrumentation Boxes in Back of the 3-ft Antenna (15.4 GHz) and the 18-in. Antenna (35 GHz)	15
5. Wiring Distribution Diagram for the Instrumentation Box of the 35-GHz Radiometer	16
6. Photograph Showing the Assembled Components in the 35-GHz Instrumentation Box	17
7. Wiring Diagram for Power Supply Assembly	18
8. Chart of an Antenna Drift Pattern Through the Sun	19

## Tables

1. Dates When Systems at Various Frequencies Became Operational at the Sagamore Hill Radio Observatory	9
--------------------------------------------------------------------------------------------------------	---

## Improved 35 GHz Radiometer for Solar Burst Measurements

### 1. INTRODUCTION

In the mid-1960's, the Solar Radio Section of the Radio Astronomy Branch at Air Force Cambridge Research Laboratories (AFGL's predecessor) under the leadership of Mr. John Castelli began routine daily radio measurements of the sun at a variety of fixed frequencies in the decimeter-centimeter wavelength range. Eventually, whole-sun patrol observations were carried out from sunrise to sunset at nine frequencies from 245 MHz to 35 GHz at the Sagamore Hill Observatory at Hamilton, Massachusetts. The dates when the Sagamore Hill radiometric systems at the various frequencies became operational are given in Table 1. A view of the Sagamore Hill solar patrol station is shown in Figure 1.<sup>1</sup>

The solar radio patrol at Sagamore Hill, like most whole-sun patrols, measures the flux density of the quiet sun (once a day, usually at local noon) and of bursts (often far more intense than the quiet-sun radiation). Because of the large dynamic range of solar radio signals, receiver nonlinearity (occurring principally in the video detector following the intermediate-frequency amplifier) can be a significant problem. It is most severe at meter and decimeter wavelengths. For example, at 250 MHz the quiet-sun flux density ( $S_{qs}$ ) is about 15 sfu, while the peak

(Received for publication 25 August 1981)

1. Castelli, J. P., Aaronson, J., Guidice, D. A., and Straka, R. M. (1973) The solar radio patrol network of the USAF and its application, Proc. IEEE, 66:1307-1312, AFCRL-TR-74-0007, AD 774169.

flux density of the largest bursts ( $S_{lb}$ ) can reach 500,000 sfu [ $1 \text{ sfu} = 10^{-22} \text{ W/m}^2 \text{ Hz}$ ]. For centimeter wavelengths, the problem is less severe, but still important, (see Figure 2). For short centimeter and millimeter wavelengths, the dynamic range of solar signals further contracts, and nonlinearity is no longer a critical problem. For example, at 15 GHz,  $S_{qs} \approx 500 \text{ sfu}$ , while  $S_{lb}$  never exceeds 50,000 sfu.

At millimeter wavelengths, the main problem for whole-sun patrol observations is radiometer sensitivity. The necessity of viewing the "whole sun" with an antenna whose beamwidth is several solar diameters results in a small antenna collecting area and thereby a relatively small solar signal.

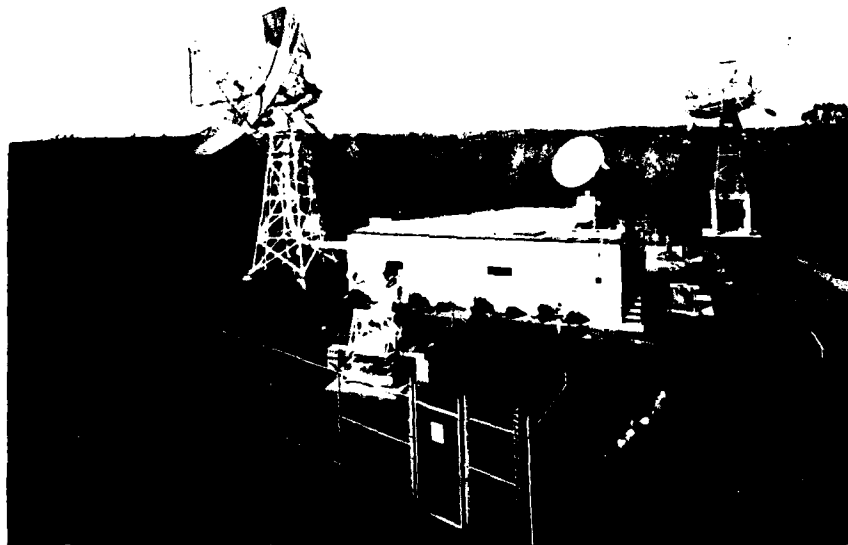


Figure 1. A View of the Sagamore Hill Solar Radio Patrol Station

Table 1. Dates When Systems at Various Frequencies Became Operational at the Sagamore Hill Radio Observatory

Frequency (MHz)	Date
245	Feb 1969
410	Apr 1971
606	Jan 1966
1415	Jan 1966
2695	Jan 1966
4995	Jan 1966
8800	Jan 1966
15,400	Jan 1968
35,000	Nov 1968

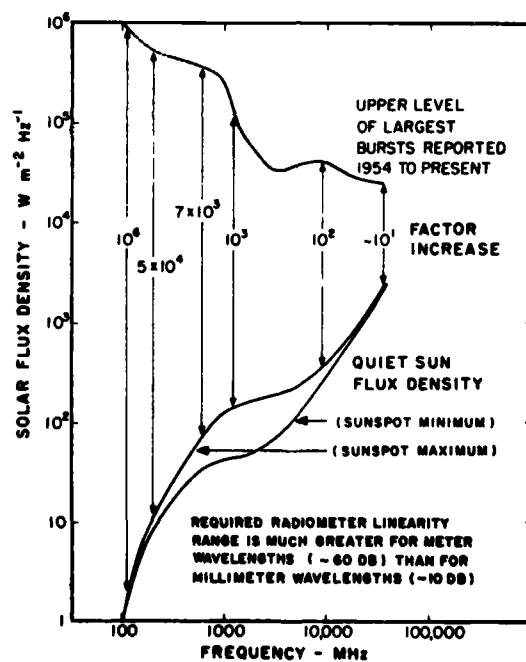


Figure 2. Upper Level of Largest Burst Flux Density Over the Microwave Range in Comparison to Quiet-sun Flux Densities

If the sun does not appear as nearly a point source to the antenna, the determination of true flux density for the quiet sun requires a correction factor which considers beam shape and source brightness distribution.<sup>2</sup> A discrepancy in measuring the flux density of bursts also arises when the antenna beamwidth is less than several times the solar diameter. Since the antenna routinely follows the center of the sun (standard patrol procedure), the measured or apparent flux density of a burst occurring towards the sun's limb is less than it would be if it occurred at the sun's center. Ordinarily in whole-sun patrols, the problems are avoided by reducing antenna size to make the beamwidth at least 3 to 5 times the sun's diameter. At 35 GHz, a compromise is made between radiometer sensitivity and measurement accuracy; a 1.5-ft parabolic antenna is used, giving a half-power beamwidth of about 1.4°.

The original 35-GHz radiometer system at Sagamore Hill had an 8-MHz IF bandpass centered at 30 MHz, the same as that used for the other patrol frequencies. Also, the mixer-preamplifier of the original 35-GHz system, state of the art for the early 1960's, had a noise figure of about 13 dB. These receiver parameters combined with the small collecting area of the 1.5-ft parabola resulted in a system sensitivity of about 40 sfu.

The original radiometer was thus unsuitable for measuring even the peak flux density at 35 GHz of small (< 50 sfu) impulsive bursts and almost all gradual rise and fall (GRF) bursts. It was also unsuitable for measuring the time profile of the 35 GHz radiation of bursts of moderate (50-500 sfu) peak flux density at 35 GHz. Since the 35 GHz time profile was very important in studying the spectral (flux density vs frequency) development of a radio burst with time, modifications had to be made to improve the sensitivity of Sagamore Hill's original 35 GHz radiometer system.

## 2. RADIOMETER IMPROVEMENTS

### 2.1 Design Improvements

The sensitivity of a radiometric system is defined by the minimum detectable temperature change,  $\Delta T(\text{rms})$ , given by:

$$\Delta T(\text{rms}) = \frac{C T_{\text{sys}}}{\sqrt{B \tau}} \quad (1)$$

2. Guidice, D. A., and Castelli, J. P. (1971) The use of extraterrestrial radio sources in the measurement of antenna parameters, IEEE Trans. Aerosp. & Elec. Sys. AES-7:226-234, AFCRL-71-0345, AD 725800.

where  $C$  is a constant depending upon the type of modulation used in temperature comparison,  $T_{\text{sys}}$  is the system noise temperature,  $B$  is the pre-detection bandwidth and  $\tau$  is the post-detection time constant.

For a total power system (no comparison switching), we have  $C = 1$ . For a Dicke system (comparison switching between the antenna line and a constant-temperature matched load) with a square-wave modulation (switching) and square-wave demodulation, we have  $C = 2$ , since the input signal is connected to the receiver half the time. When a narrow-band filter (centered at the modulation frequency) is inserted into the post-detection portion of the receiver to avoid the danger of overloading from extraneous noise, sine-wave demodulation (instead of square-wave) results, and we have  $C = \pi/\sqrt{2} = 2.22$ .<sup>3</sup> Since the sensitivity loss imposed by this approach is only 11%, it is customarily used in Dicke-type systems. This is the approach used in our Sagamore Hill 35 GHz radiometer.

The system noise temperature is given by:

$$T_{\text{sys}} = T_{\text{rec}} L + T_{\text{ext}} \quad (2)$$

where  $T_{\text{rec}}$  is the noise temperature of the receiver,  $L$  is the r.f. loss factor ( $L \geq 1$ ), and  $T_{\text{ext}}$  is the equivalent temperature of external (prereceiver) noise sources.  $T_{\text{ext}}$  can be taken as roughly the average of the comparison-load temperature ( $T_{\text{load}}$ ) and the antenna-line temperature ( $T_{\text{ant}}$ ). The latter can vary significantly according to whether the antenna is pointing at the sky or the sun. The receiver noise temperature is given by:

$$T_{\text{rec}} = (F_n - 1) T_o = (F_n - 1) 290 \text{ K} \quad (3)$$

where  $F_n$  is the receiver noise figure and  $T_o = 290 \text{ K}$  by IEEE definition ( $T_o$  is roughly room temperature). In the case of the 35 GHz radiometer, where the mixer accepts both the upper and lower sideband,  $F_n$  is the double-sideband (DSB) noise figure.

Combining Eqs. (1) and (2), the relationship for minimum detectable temperature is given by:

$$\Delta T(\text{rms}) = C \frac{(T_{\text{rec}} L + T_{\text{ext}})}{\sqrt{B \tau}} \quad (4)$$

The relation between the "antenna temperature" measured by a radiometer observing a radio source of flux density  $S$  (when the antenna beamwidth is several times the angular extent of the source) is given by the expression:

3. Kraus, J.D. (1966) Radio Astronomy, McGraw-Hill, New York, pp 250-251.

$$S = \frac{2kT_A}{A_e} \quad (4)$$

where  $S$  is the flux density (in  $\text{W/m}^2 \text{ Hz}$ ),  $k$  is the Boltzmann's constant ( $1.38 \times 10^{-23} \text{ J/K}$ ),  $T_A$  is the antenna temperature (in K), and  $A_e$  is the effective area of the antenna.

Since the minimum detectable temperature change one tries to measure with a radiometer is the change in antenna temperature, we can define another term, minimum detectable flux density,  $\Delta S(\text{rms})$ , by the relation:

$$\Delta S(\text{rms}) = \frac{2k}{A_e} \Delta T(\text{rms}) = \frac{2k}{A_e} \frac{C T_{\text{sys}}}{\sqrt{B \tau}} \quad (6)$$

or

$$\Delta S(\text{rms}) = \frac{2k}{A_e} \frac{C(T_{\text{rec}} L + T_{\text{ext}})}{\sqrt{B \tau}} \quad (7)$$

As introduced in the Introduction, 40 sfu was unsatisfactory as the sensitivity or minimum detectable flux density of the old 35 GHz radiometer system. By examining Eq. (5), one can see where improvements can be made to reduce  $\Delta S(\text{rms})$ .

The constants  $k$  and  $C$  cannot be changed.  $A_e$  cannot be made larger (that is, by using a larger antenna) because this would result in a narrower antenna beam. Since the  $1.4^\circ$  beamwidth of the antenna (18-in. diameter parabola) of the old Sagamore Hill 35 GHz radiometer is already stretching the lower limit of the beamwidth needed (3-5 times the sun's diameter,  $0.5^\circ$ ) to avoid the flux density measurement errors discussed in Section 1, antenna size cannot be increased.

$T_{\text{ext}}$  relates mainly to external noise temperatures (sky, sun) not readily controllable by the radiometer designer; hence, no means of improvement can be found here.

The time constant  $\tau$  cannot be increased beyond its 1-sec value (as in the old system) because we need to make the 35 GHz radiometer responsive to flux density changes occurring on a time scale of this order. (The radiometers at the other frequencies of the Sagamore Hill patrol all have a 1-sec integrating time.) Also, other non-radio instruments measuring electromagnetic radiation from the sun (for example, hard x-rays) typically have measurement response times on the order of a second or less. We want the radiometers of our radio patrol to have similar time-resolution capabilities so we can compare measured variations in the radiation from solar bursts at different portions of the electromagnetic spectrum.

From the above discussion, we see that receiver noise temperature ( $T_{\text{rec}}$ ) and predetection bandwidth ( $B$ ) are the only parameters that can be upgraded to give

improved sensitivity performance. Fortunately, the components needed to obtain the required improvements have been developed over the last few years and are commercially available. These include low-noise mixers with average double-sideband (DSB) noise figures (over a wide band) on the order of 4 to 6 dB at 35 GHz and intermediate frequency (IF) amplifiers with bandpasses covering a frequency range from tens of megahertz to 500 or even 1000 MHz. These devices are typically configured as (1) a mixer-preamplifier which converts the DSB signal at 35 GHz to the IF band and imparts a fixed IF gain of about 20 to 30 dB and (2) a main IF amplifier which imparts a gain (typically) of about 40 to 80 dB maximum with an electronic or mechanically variable gain control of about 0-20 dB.

In our new 35 GHz system, we make use of a mixer-preamplifier having a 4 dB nominal (and about a 6 dB actual) DSB noise figure, a 50 to 500 MHz bandpass, and a 20 dB IF gain. The main IF amplifier (with a matching 50 to 500 MHz bandpass) has about 45 dB of gain with a 0-20 dB electronic gain control.

The advertised DSB noise figure of the mixer-preamplifier for  $35.0 \pm 0.5$  GHz was 4 dB. Vendor measurements using a limited passband (70 MHz) with the local oscillator at various frequencies within the 34.5 to 35.5 GHz specified range show a meeting (individually) of the 4.0 dB noise figure specifications over the 34.5-35.5 GHz range. However, this procedure is not the same as setting the local oscillator at 35.0 GHz and measuring the overall noise figure for a  $\pm 500$  MHz bandpass. From our radiometric measurements (a less precise approach) we estimated the average noise figure (out to  $\pm 500$  MHz) to be about 6 dB.

## 2.2 Block Diagram and Wiring Diagrams

Figure 3 shows a block diagram of the improved 35 GHz radiometer for the Sagamore Hill Radio Observatory. The components to the left of the heavy dashed line are contained in an instrumentation box located in back of the 18-in. parabolic antenna mounted on the MP61B solar tracking unit, (see Figure 4). The remaining components of the 35 GHz system (the so-called radiometer "back-end"), consisting principally of the lock-in amplifier and chart recorders, are housed in a standard 19-in. rack within the Solar Building.

Figure 5 shows the wiring distribution diagram for the instrumentation box. Figure 6 is a photograph showing the internal three-dimensional layout of the instrumentation box. Figure 7 is the wiring diagram for the power supply assembly which supplies dc voltages and control signals to various functional units of the radiometer. A parts list of the components in the new 35 GHz radiometer is given in Appendix A.

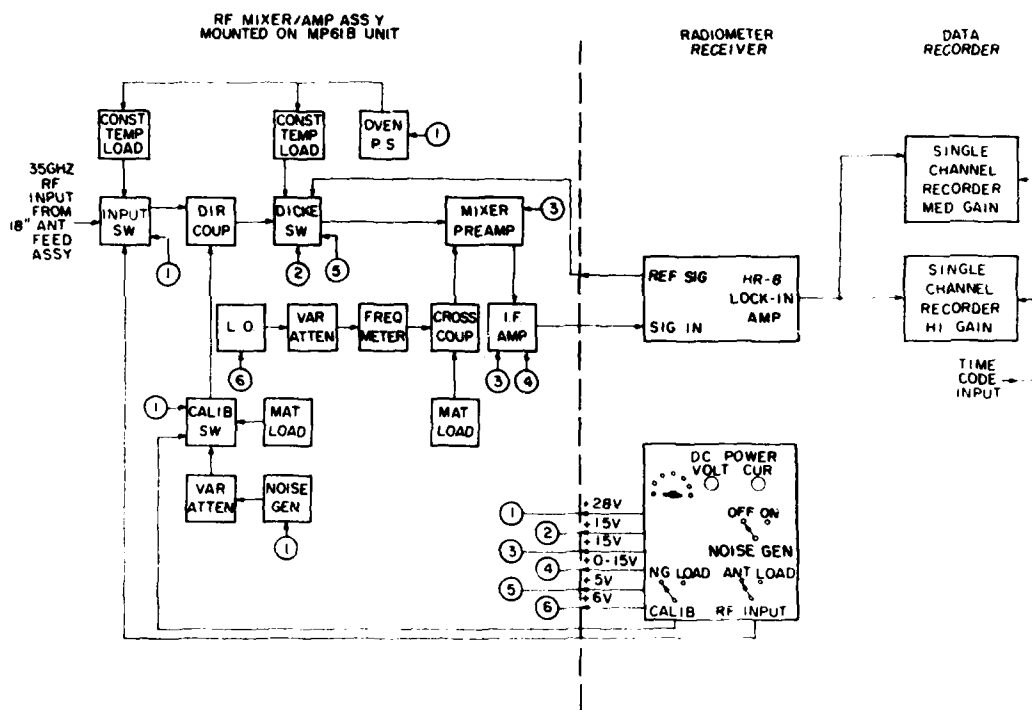


Figure 3. Block Diagram of the Improved 35 GHz Radiometer

### 2.3 Sensitivity Calculations for the New System

Before calculating the expected sensitivity of the new 35 GHz radiometer, we needed to obtain the values of the various factors in Eq. (4). Some values are derived from the system configuration, others from assumptions or component measurements.

Since the radiometer uses Dicke switching with square-wave (modulation and sine-wave demodulation, the constant  $C$  equals 2.22 (see Section 2.1).

The losses between the antenna and the input of the mixer-preamplifier (including the input switch, directional coupler, Dicke switch, and several waveguide runs) were measured and found to be roughly 2.0 dB. Thus, the loss factor  $L$  (a number greater than one, as we define it in the sensitivity equation) is 2 dB or 1.585.

The double sideband noise figure  $F_n$  is 6.0 dB or 3.98. Therefore, the receiver noise temperature  $T_{rec} = (F_n - 1)T_o = (3.98 - 1)290K = 864K$ .

The external noise temperature  $T_{ext}$  depends to some extent on what the antenna observes at the time of the measurements. If it were pointed at the sun,  $T_{ext}$  would be roughly equal to the average of the antenna temperature of the sun



Figure 4. Photograph Showing the Instrumentation Boxes in Back of the 3-ft Antenna (15.4 GHz) and the 18-in. Antenna (35 GHz)

(about 500 K, derived later in this section) and the comparison-load temperature (about 350 K); thus,  $T_{\text{ext}}$  would equal about 425 K. In determining radiometer sensitivity, however, we are interested in a quality of the receiver and want to minimize the influence of external sources. Therefore, we point the antenna at the sky (away from the sun) for the sensitivity measurements. Hence,  $T_{\text{ext}}$  will be roughly equal to the average of the sky-background temperature (about 50 K) and the comparison-load temperature (about 350 K);  $T_{\text{ext}} \approx 200$  K.

The bandpass of our receiver runs from about 50 MHz to about 450 MHz; hence, we take the bandwidth  $B$  as 400 MHz. As discussed in Section 2.1, the time constant or integrating time  $\tau$  is 1 sec.

Putting the values derived above into Eq. (4), we have:

$$\Delta T(\text{rms}) \approx C \frac{T_{\text{rec}} L + T_{\text{ext}}}{B \tau} = 2.22 \frac{864(1.585) + 200}{\sqrt{400 \times 10^6 (1)}},$$

$$\Delta T(\text{rms}) \approx 0.175 \text{ K}.$$

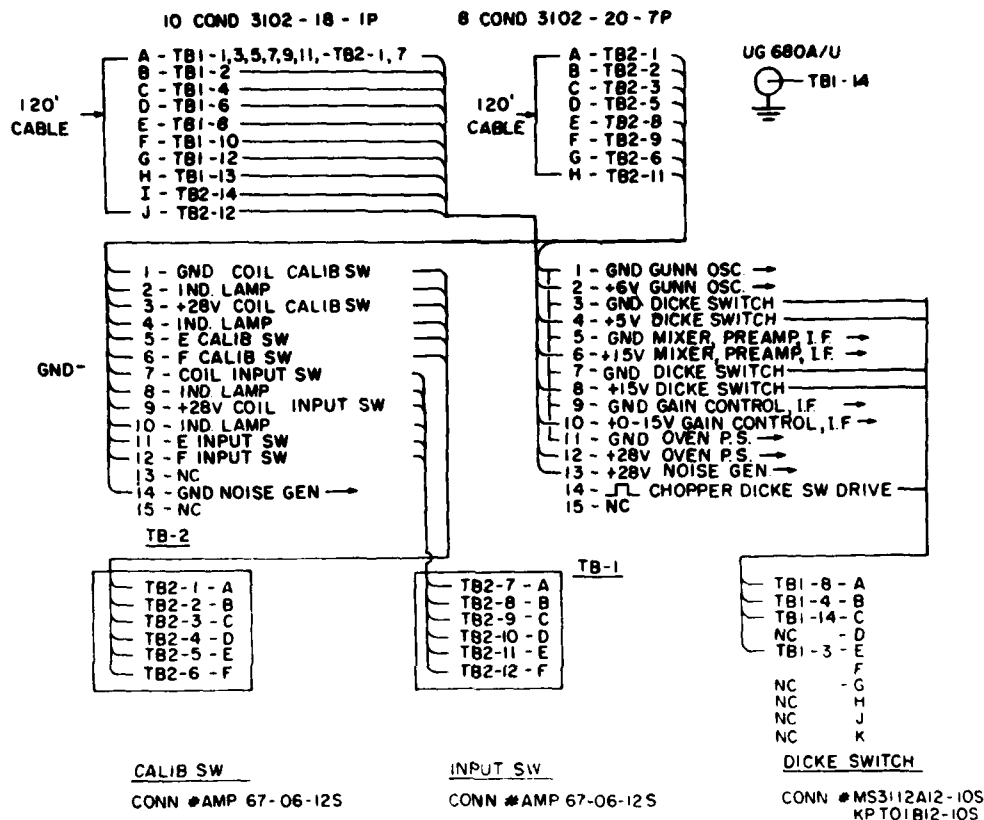


Figure 5. Wiring Distribution Diagram for the Instrumentation Box of the 35 GHz Radiometer

To check out the actual sensitivity of the new 35 GHz radiometer, we must employ a parameter we can measure on a chart record; that is, the peak-to-peak noise fluctuation. The relationship between  $\Delta T(\text{rms})$  and  $\Delta T(\text{p-p})$  is:

$$\Delta T(\text{p-p}) = 6 \Delta T(\text{rms}). \quad (8)$$

Thus, the calculated value of  $\Delta T(\text{p-p})$  is 1.05 K. For the experimental determination of sensitivity, we measure  $\Delta T(\text{p-p})$  in chart divisions on an analog record. In addition, we must derive a scale (temperature [in K] per chart division) for the record.



Figure 6. Photograph Showing the Assembled Components in the 35-GHz Instrumentation Box

We take a drift through the sun to obtain a chart record of antenna temperature whose value we derive from Eq. (5) and an assumed value of 2000 sfu ( $1 \text{ sfu} = 10^{-22} \text{ W/m}^2\text{Hz}$ ) for the quiet-sun flux density at 35 GHz. This is the flux density value used in the past for 35 GHz patrol operations. At decimeter and long-centimeter wavelengths, the sun's slowly varying component (SVC) causes the quiet-sun flux density to vary over a range of several times its sunspot-minimum background level. At millimeter wavelengths (35 GHz), the SVC is relatively much smaller (only about five percent of the background level). Hence, for the temperature-scaling accuracy needed for the  $\Delta T(p-p)$  measurement, we can neglect any SVC variations in the sun's 35 GHz emission.

The effective area  $A_e$  of our 18-in. (0.457 m) parabolic antenna is equal to  $\eta_a A_p$ , where  $\eta_a$  is the aperture efficiency (taken as 0.5) and  $A_p$  is the physical area. Since  $A_p = (\pi/4) (0.457 \text{ m})^2 = 0.164 \text{ m}^2$ , the effective area  $A_e = 0.082 \text{ m}^2$ .

At 35 GHz, the radio emission (flux density) of the sun is attenuated by passage through the earth's atmospheric gases. As long as it is not raining, the atmospheric attenuation is not a serious problem, but it does lower the solar signal level arriving at the antenna, especially when observing on overcast days at the low elevation angles (high zenith angles) that go with winter measurements. For the climatic conditions and zenith angles of the observations during radiometric testing, we estimate the atmospheric attenuation to be -0.5 dB, or a factor 0.89. Thus, the signal

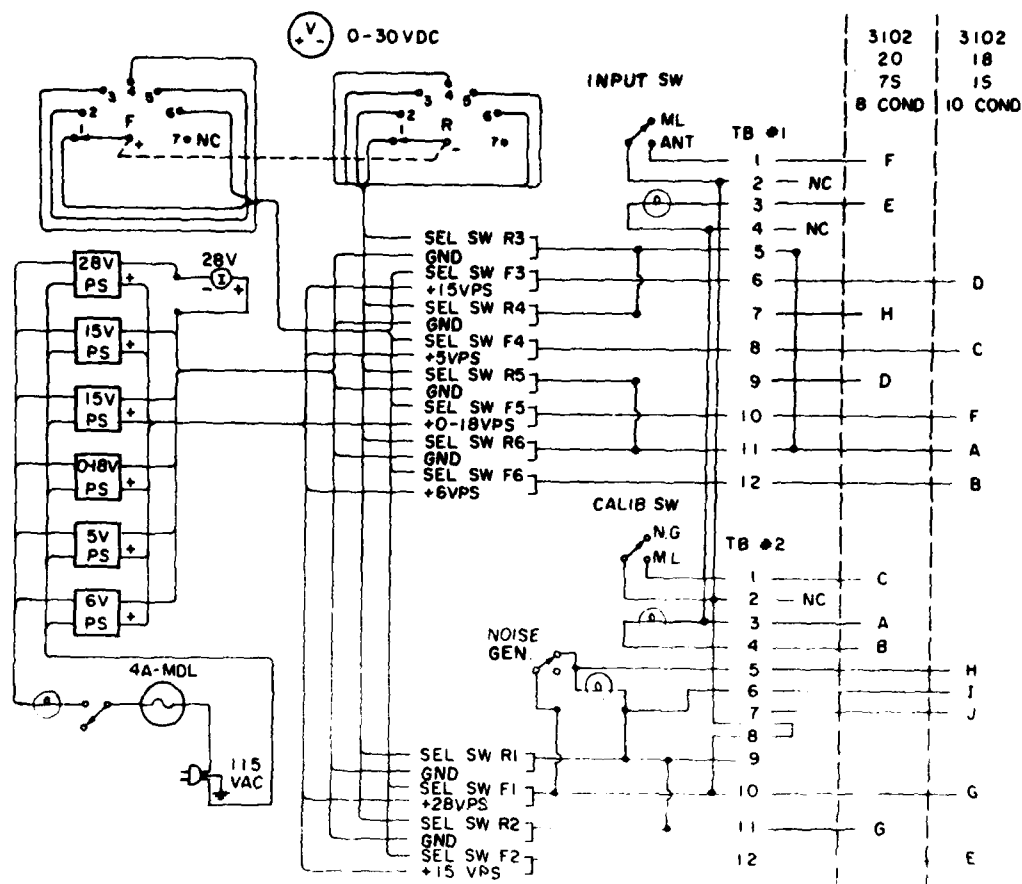


Figure 7. Wiring Diagram for Power Supply Assembly

strength (flux density) from the sun presented to the antenna is  $0.89 \times 2000$  siu or 1780 sfu.

Using Eq. (5) and the parameters derived above, we have:

$$T_A = \frac{S A_e}{2k} = \frac{1780 \times 10^{-22} (0.082)}{2 (1.38 \times 10^{-23})}$$

$$\approx 529 \text{ K.}$$

To measure the temperature scale, we obtain a drift curve through the sun, (see Figure 8). The amplitude difference between the top of the drift curve and the baseline (sky background) is 46 chart divisions in this case. Hence, the temperature scale of the chart is 529 K/46 div or about 11.5 K/div.

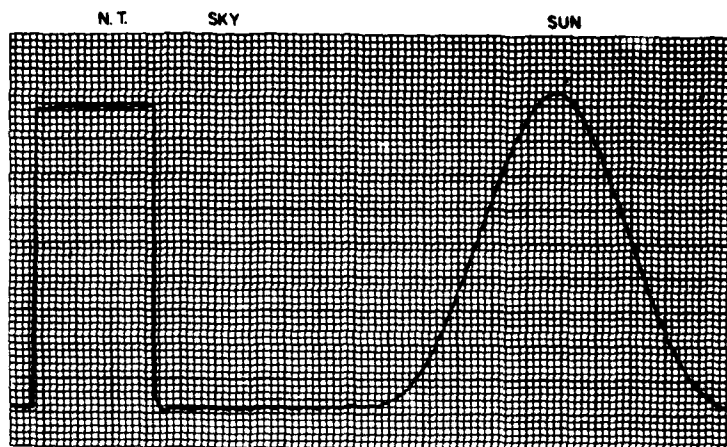


Figure 8. Chart of an Antenna Drift Pattern Through the Sun. The noise-tube calibration is also shown

The peak-to-peak noise fluctuation amplitude is roughly 0.1 div on the chart. This is difficult to read (note Figure 8). However, later in the record (not shown in Figure 8), we increased the recorder gain by 10, measured the peak-to-peak fluctuation amplitude (about one chart division) in sky background (baseline), divided the higher-gain observation by 10, and obtained about the same result.

To obtain  $\Delta T(p-p)$  we multiply the peak-to-peak noise fluctuation (in chart div) by the temperature scale,  $0.1 \text{ div} \times (11.5 \text{ K/div})$ . We obtain a measured  $\Delta T(p-p)$  considering the difficulty in estimating the peak-to-peak noise fluctuation in chart division.

We could have also derived the temperature scale for the  $\Delta T(p-p)$  measurement from the measured excess noise figure of the solid-state noise generator and the losses in the variable attenuator, waveguide (calibration) switch, and directional coupler (see Figure 3). The temperature scale derived by this approach turned out to be about 12 K/div, agreeing with the results of the method described above.

We can derive the minimum detectable flux density  $\Delta S(rms)$  by a relationship analogous to Eq. (5),

$$\Delta S(rms) = \frac{2kk}{A_e} \Delta T(rms). \quad (9)$$

Using the previously derived  $A_e = 0.082 \text{ m}^2$  and taking  $\Delta T(p-p) = 1.1 \text{ K}$  and  $\Delta T(rms) = 0.18 \text{ K}$ , we have  $\Delta S(rms) = 0.60 \times 10^{-22} \text{ W/m}^2 \text{ Hz}$  or  $0.60 \text{ sfu}$ . Since the same peak-to-peak and rms relationship [Eq. (8)] holds for flux density, we also have  $\Delta S(p-p) = 6 \Delta S(rms) = 3.6 \text{ sfu}$ .

### 3. NEW CAPABILITIES

#### 3.1 For the 35 GHz Patrol

With a  $\Delta S(\text{rms})$  of 0.6 sfu [ $\Delta S(\text{p-p})$  of 3.6 sfu], the ability of the 35 GHz radiometer to detect and measure the flux density of small solar bursts is no longer limited by receiver sensitivity. The factor now limiting burst measurement is some small inherent fluctuations in the solar signal received by the radiometer. The enhanced fluctuations, which are seen when the system views the sun (larger than when the system "views" sky background or a matched-load termination), are noticeable on the analog chart record. The "sun-viewing" fluctuations are of the order of 3-5 sfu (sometimes 5-10 sfu).

The small additional fluctuations could be due to short time-scale changes in the actual flux density of the quiet-sun's 35 GHz emission (4 sfu is only 0.2 percent of the quiet-sun's 2000 sfu) or could be caused by attenuation variation in the intervening terrestrial atmosphere (between the sun and the receiving antenna). Probably, the result is a combination of the two effects. Some days the phenomenon is more noticeable than others; this tends to support the case for atmospheric attenuation being the main cause.

A radiometer patrol at one frequency can detect, on its own, bursts of the order of one-half the peak-to-peak noise fluctuations. If one has knowledge by some other means (from another patrol frequency, for example) of the presence and approximate shape (simple) of a burst, one can make a measurement of its flux density to a level of about twice the  $\Delta S(\text{rms})$  level of the radiometer. This is assuming no disturbance of the apparent quiet-sun level, that is, no changes in atmospheric attenuation, no wind-induced antenna motions, no antenna temperature variations due to ground pickup from a sidelobe.

In rough terms, the old 35 GHz radiometer system was capable of detecting measuring bursts down to about a 50-100 sfu level, the new system down to about a 5-10 sfu level. Let us briefly see what this new sensitivity allows the 35 GHz patrol to accomplish.

On generally clear days, it allows the measurement of the 35 GHz flux density of many gradual rise and fall (GRF) bursts. While the majority of GRF's are probably less than 10 sfu at 35 GHz, significant numbers of them reach a level of 20 or even 30 sfu.

Even on days with some atmospheric variations, one can measure the peak flux density of small impulsive bursts (10 to 25 sfu) at 35 GHz. For somewhat larger impulsive bursts (25 to 100 sfu, for example), one can measure the general time profile of a burst, determine its rise and decay times, and characterize its morphology at 35 GHz.

For the larger impulsive or complex bursts, one can obtain the complete time development (burst flux density vs time) at 35 GHz. At present there is a difficulty in reading the analog chart records because of the compression of the time scale (60 sec in 1/2 in.); however, a new automated digital data processing system coming to Sagamore Hill will alleviate the chart reading problem.

The automation system, which will be similar to those used at the other RSTN stations (Palehua, Hawaii and Learmonth, Australia), will give a digitized read-out (printout, if one wants it in that form) of burst flux density at 1-sec time intervals. Hence, we will have the means to take full advantage of the improved sensitivity of the new 35 GHz radiometer.

### 3.2 For the Solar Radio Patrol as a System

As a result of the improved-sensitivity 35 GHz radiometer, allowing detailed observations of burst spectra out to millimeter wavelengths, we open the possibility of exploring several exciting areas of solar physics through analysis and interpretation of radio spectral data. In some (but not all) cases, another system improvement, automated data processing, is needed so that we can obtain a burst flux-density value at each patrol frequency (245 MHz to 35 GHz) during each second of the burst. In the next several paragraphs, we examine several of these areas of exploration.

#### 3.2.1 TIME DEVELOPMENT OF SPECTRA OF SELECTED LARGE BURSTS

The solar radio patrol with its enhanced upper-frequency capability can show the spectral development (with time) for individual large complex bursts. These very large bursts often have accompanying large-scale particle acceleration. In the case of high-energy ( $E \gtrsim 10$  MeV) proton events, the resultant protons upon reaching the earth cause polar cap absorption and other geophysical phenomena disruptive to Air Force systems and operations.

A particular area of interest for energetic-particle events is the time (and active region location) of the particle acceleration in a burst. The study of several large proton events has uncovered a so-called "hinging" effect. During the flux-density-increasing portion of the burst, flux density at the upper end (15-35 GHz) of the radio spectrum increases much more rapidly than at the lower end (5 GHz or below). [Upper-end intensity flips up rapidly while lower-end intensity stays roughly constant, making the spectrum appear to be "hinged" at lower frequencies.] In the subsequent flux-density-decreasing portion of the burst, there seems to be a systematic flux density decrease throughout the microwave spectral range without any rapid change in spectral shape.

The existence of the "hinging" effect and its association with proton energy-spectrum parameters lends support to the concept that particle acceleration takes place in the impulsive or "flash" phase of a large burst. Yet other evidence (for example, the existence of long-lasting, low peak flux density bursts producing significant numbers of protons without a strong impulsive phase) leads to the need for a second-stage gradual process to be responsible for proton acceleration to the 10-100 MeV energy range. It is hoped that further study of the spectral development of selected large bursts will produce a better understanding of particle acceleration processes in flare-bursts.

### 3.2.2 TIME DEVELOPMENT OF SPECTRA OF MANY SIMPLE BURSTS

Radio emission from the very large bursts often consists of many overlapping components that can come from various active region locations (which might have quite different physical properties). Although the study of the largest bursts as individual events is important, because of their rarity they contribute little in a statistical sense to the study of burst characteristics in general.

For an investigation of the statistics of burst-region parameters observations of many moderate-intensity relatively-simple radio bursts might be more rewarding. From measurements of burst flux density vs frequency at 1-sec intervals (now with sufficient flux density resolution at the upper frequencies), one can, for large numbers of bursts, characterize spectral shape changes (with time) in different phases of a burst, relate rise or decay times in different frequency regimes, and so on. The study of any interrelationships found can lead to a better determination of the typical physical properties of the radio-emitting regions of flare-bursts.

### 3.2.3 CORRELATION OF HARD X-RAY SPECTRA WITH MICROWAVE SPECTRA

Hard x-ray and microwave emissions from solar flare-bursts are being analyzed to investigate the nature of the impulsive and gradual emission sources in bursts. The development with time of the spectra (intensity vs energy range) of the hard x-ray emission from certain bursts will be compared with the development with time of the spectra (flux density vs frequency) of the microwave emission from these same bursts. Because of the enhanced sensitivity at the upper end of the microwave spectrum (the most important end in regard to the study of acceleration mechanisms) brought about by the improved 35 GHz radiometer, it is expected that significant radio-spectral findings will be uncovered. Analytic results will be used to develop a better understanding of energetic-particle (electrons and protons) accelerating mechanisms operating in solar flare-bursts.

### 3.2.4 HIGH-FREQUENCY SHARP-CUTOFF BURSTS

A class of impulsive, low-to-moderate intensity radio bursts has been found with peculiar peak flux density spectra; a very high spectral maximum (9 to 15 GHz or higher) with a very sharp cutoff on its low-frequency side (flux density reduced to less than a few percent of its spectral maximum in less than an octave of frequency range). An investigation has shown that clusters of these bursts are associated with active regions that give rise to large flare-bursts that produce energetic proton events. This phenomenon was first noticed in the region McMath 11976, which produced the 2 to 7 August 1972 proton events.<sup>4</sup> A search of worldwide solar radio patrol records for 1966-1972 uncovered 56 occurrences of clusters of these sharp-cutoff bursts that could be identified with a particular active region. Two-thirds of these regions produced a proton flare within 72 hours (before or after) of the observation of the sharp-cutoff bursts. In general, the greater the proton-event production from an active region, the greater the likelihood of its having sharp-cutoff bursts.

With the old 35 GHz radiometer and its poor sensitivity, we could not learn much about the mm-wavelength emission of these sharp-cutoff bursts. With the new radiometer we can measure their 35 GHz peak flux density, which may be rather low. (For most sharp-cutoff bursts, peak flux density at spectral max [9 to 15 GHz] is less than 50 sfu and often less than 25 sfu; fortunately, flux density on the high-frequency side decreases less precipitously.) The new 35 GHz system can now provide information beyond the spectral-maximum frequency and also allow better determination of that frequency.

We should note that, of the four areas of exploration discussed in this section, it is only in this last area (sharp-cutoff bursts) that we do not, strictly speaking, need to have automated data processing (with its high time resolution) to make use of the improved sensitivity of the 35 GHz system. (This exploration area involves peak flux density spectra, not variation of the spectra with time.) However, even for this application, automated retrieval of peak flux density values is helpful.

## 4. CONCLUSION

In conclusion, one can see that there are numerous advantages of an improved-sensitivity 35 GHz radiometer in a whole-sun solar radio patrol. We therefore recommend that, wherever possible, such a radiometer be added to the other stations of the Air Force's Radio Solar Telescope Network.

4. Castelli, J. P., Guidice, D. A., Forrest, D. J., and Babcock, R. R. (1974) Solar Bursts at  $\lambda = 2$  cm on 31 July 1972, J. Geophys. Res. 79:889-894. AFCRL-TR-74-0163, AD 779114.

## Appendix A

### 35 GHz Solar Radiometer Parts List

<u>Quantity</u>	<u>Part</u>	<u>Manufacturer</u>
1	Power Supply, 5 VDC, $\pm 0.5$ V, 0.25 A, Model 6130 PVBGT25 (for Dicke Switch)	Acopian
1	Power Supply, 6 VDC, $\pm 0.5$ V, 0.9 A, Model 6130 PVA6MT490 (For Gunn. Osc.)	Acopian
2	Power Supply, 15 VDC, $\pm 1.0$ V, 0.2 CA Model 6130 PVB15GT20 (for Dicke Sw., Mixer)	Acopian
1	Power Supply, 28 VDC, $\pm 0.5$ V, 5.0 A, Model A-28MT500SW (for Mat. Load Oven)	Acopian
1	Power Supply 0-18 VDC, 400 mA, Model VA018NT40 (for Preamp Gain Control)	Acopian
1	Gunn Effects Osc., Model VSA 9010	Varian
2	Attenuator, Variable, Model A520	TRG-Alpha Ind.
1	Mixer Preamp, Model F35-U	Space-Kom
1	IF Amplifier, Model U25D	Space-Kom
1	Dual Load, Temp. Control, Model A583	TRG-Alpha Ind.
1	Noise Gen., Model No. 7350W	Microwave Semicond. Corp.
2	Waveguide Switch, Model DBD-612AE-2	Systron-Donner
1	Dicke Switch, Model 570S1	Electro-Mag. Sciences
1	Parabolic Antenna/Feed, Model A802-18	TRG-Alpha Ind.
1	Wavemeter, Model A551	TRG-Alpha Ind.

<u>Quantity</u>	<u>Part</u>	<u>Manufacturer</u>
1	Cross Coupler, Model DBD-631-15	Svstron-Donner
1	Directional Coupler, 13 DB, Model A 559-13	TRG-Alpha Ind.
4	Termination, Model A580	TRG-Alpha Ind.
6	H-Plane Bends, 90°, Model A670	TRG-Alpha Ind.
2	H-Plane Bends, 45°, Model A665	TRG-Alpha Ind.
2	E-Plane Bends, 45°, Model A675	TRG-Alpha Ind.
6	E-Plane Bends, 90°, Model A660	TRG-Alpha Ind.
2	Twists, 90°, Left Hand, Model A681RH	TRG-Alpha Ind.
1	Connector, KPT06E-12-10S (10 Pin) (for Dicke Switch)	Cannon
1	Connector, 3106-18-1P (10-Pin)	Amphenol
1	Connector, 3106-18-1A (10-Pin)	Amphenol
1	Connector, 3102-18-1P (10-Pin)	Amphenol
1	Connector, 3102-18-15 (10-Pin)	Amphenol
1	Connector, 3106-20-7P (8-Pin)	Amphenol
1	Connector, 3106-20-7S (8-Pin)	Amphenol
1	Connector, 3102-20-7P (8-Pin)	Amphenol
1	Connector, 3102-20-7S (8-Pin)	Amphenol
1	Connector, 67-01-J12-7S (7-Pin)	Amphenol
2	Adapter, Model 501-1 (for IF Amplifier)	OSM
1	Adapter, 879-5 DLA900-78-M-977 (for IF Amplifier)	OSM
1	Connector UG30E/U "N" FEEDTHRU	Amphenol
1	Adapter, PN2088-0001-31 DLA900-78-M U349 (for Mixer/Preamp to IF Amp)	OSM
1	Connector UG201 A/U "N" to BNC	Amphenol
1	Cable, 120 Feet, 10 Cond/Shield, FSN 6145-818-4653 (Power Cable)	Belden
1	Cable, 120 Feet, 8 Cond/Shield	Belden
1	Connector, UG680 A/U ?N? Chassis	Amphenol
1	Cable, 120 Feet, RG-9 (for IF Amp. to HR-8)	Belden
1	Cable, 120 Feet, RG-9 (for Switch Driver)	Belden
1	Cable, 12 in., RG-55 (for IF Amp.)	Belden
1	Preamp Box, 23 in. X 14 in. X 10 in.	Zero Mfr. Co.
1	Lamp Socket, 115 V, Neon (for A.C.)	Gen. Elec. Co.
2	Lamp Socket, 28 V (for Mode Sw. Indicator)	Gen. Elec. Co.
2	Barrier Term Blocks, Model 12-141 (for Power Dist.)	Cinch Co.
2	Barrier Term Blocks, 15-141	Cinch Co.
1	Meter, PN-17449, 0-30 VDC, 2-1/2" Face	Simpson

<u>Quantity</u>	<u>Part</u>	<u>Manufacturer</u>
1	Meter, PN-17405, 0-10 ADC, 2-12" Face	Simpson
1	Switch, 7 Position, 2 Gand, PA2004	CENTRALAB
1	Switch, DPST (for A. C. in)	Carling
2	Switch, DPST (for Mode Selection)	Carling
1	Fuse Holder, FHN-26-G2 30A-250 V (for Power Supply)	Buss
1	Fuse, 4 Amp, SB MDL-4 (for Power Supply)	Buss
2	Lamps, 28 V No. 327 (for Mode Indication)	Gen. Elec. Co.

